



Deposited via The University of Leeds.

White Rose Research Online URL for this paper:

<https://eprints.whiterose.ac.uk/id/eprint/108010/>

Version: Accepted Version

Article:

Birnie, C, Chambers, K and Angus, D (2017) Seismic arrival enhancement through the use of noise whitening. *Physics of the Earth and Planetary Interiors*, 262. pp. 80-89. ISSN: 0031-9201

<https://doi.org/10.1016/j.pepi.2016.11.006>

© 2016 Elsevier B.V. Licensed under the Creative Commons Attribution-NonCommercial-NoDerivatives 4.0 International <http://creativecommons.org/licenses/by-nc-nd/4.0/>

Reuse

Items deposited in White Rose Research Online are protected by copyright, with all rights reserved unless indicated otherwise. They may be downloaded and/or printed for private study, or other acts as permitted by national copyright laws. The publisher or other rights holders may allow further reproduction and re-use of the full text version. This is indicated by the licence information on the White Rose Research Online record for the item.

Takedown

If you consider content in White Rose Research Online to be in breach of UK law, please notify us by emailing eprints@whiterose.ac.uk including the URL of the record and the reason for the withdrawal request.

Seismic arrival enhancement through the use of noise whitening

Claire Birnie^a, Kit Chambers^b, Doug Angus^a

^a*Institute of Applied Geoscience, University of Leeds, UK*

^b*Nanometrics Inc., UK*

Abstract

A constant feature in seismic data, noise is particularly troublesome for passive seismic monitoring where noise commonly masks microseismic events. We propose a statistics-driven noise suppression technique that whitens the noise through the calculation and removal of the noise's covariance. Noise whitening is shown to reduce the noise energy by a factor of 3.5 resulting in microseismic events being observed and imaged at lower signal to noise ratios than originally possible - whilst having negligible effect on the seismic wavelet. The procedure is shown to be highly resistant to most changes in the noise properties and has the flexibility of being used as a stand-alone technique or as a first step before standard random noise attenuation methods.

Keywords: passive seismology, microseismic, noise whitening, noise suppression

1. Introduction

Noise is an ever present obstacle in all seismic data recordings, often preventing the user from extracting the desired signal. As such, noise suppression is one of the main topics of interest across all seismic monitoring scenarios ranging from reflection seismics (Yilmaz, 2001) to surface wave tomography (Bensen et al., 2007). In this paper we use the example of a surface microseismic monitoring scenario to introduce a noise suppression technique applicable to all seismic monitoring scenarios.

In surface passive seismic monitoring arrivals are often at or below the noise level of indi-

vidual recordings. As such noise suppression is of particular importance for monitoring of microseismic events. These events are observed in a variety of scenarios such as volcanic settings, earthquake hazard monitoring, assessing risk and containment in geo-industrial applications including geological storage of nuclear waste and carbon dioxide (CO₂), and monitoring of petroleum and mining procedures (Gambino et al., 2004; Schorlemmer and Wiemer, 2005; Maxwell, 2011; Oye et al., 2013). In general Signal to Noise Ratio (SNR) is maximised during the aquisition phase through survey design (Maxwell, 2010; Auger et al., 2013; Staněk et al., 2014). However a small number of noise suppression methods have been proposed for post aquisition, such as the application of multichannel Wiener filters (Wang et al., 2008), the use of matched filters to identify smaller events from a parent event (Eisner et al., 2008) and separating the seismic event from noise in the $\tau - p$ domain (Forghani-Arani et al., 2012).

The issue with noise suppression methods is preserving the seismic signal properties when the event is often invisible under the noise. Birnie et al. (2016) showed that realistic noise models can be built from a knowledge of the noise's covariance matrix. This work aims to reduce recorded noise to **White, Gaussian Noise (WGN)** by removing the covariance of the noise. The process of removing the covariance from a dataset is commonly referred to as noise whitening and is a well established procedure in many aspects of signal processing (Hom and Johnson, 1985; Belouchrani et al., 1997; Kessy et al., 2015). In this paper the noise whitening procedure is tested on both recorded noise, noise free synthetic waveform data and semi-synthetic datasets (datasets where recorded noise has been imposed on top of synthetic waveform data). To analyse the impact of the noise whitening, diffraction stack imaging, similar to that used by Zhebel et al. (2011), is performed on the semi-synthetic data before and after noise whitening. Using the Aquistore carbon storage site as an example, this paper demonstrates that noise whitening of seismic data results in a SNR 5 times higher, through reduction of the spatio-temporal properties of noise, whilst having negligible effect on first arrivals.

2. Theory

Noise can be separated into two categories - ambient and source-generated. Source generated noise refers to any signal that originates due to the interaction of the wavefield from the seismic source with heterogeneous earth structures (examples include ground roll and internal multiples). While the term ambient is used here to describe all noise signals independent of the seismic event, for example meteorological noise, production noise and teleseismic events. This study focusses on ambient noise, sometimes also referred to as background noise. The majority of ambient noise signals are not consistent in either space or time, further complicating noise suppression procedures. For example, passing traffic is a common source of noise with infrequent occurrences and receivers closest to the noise source most affected (Nørmark, 2011a). In a similar manner a significant drop in noise levels is observed with increasing distance from an active injection platform (Schilke et al., 2014). For non-cultural noise, Nørmark (2011b) identified varying noise levels across the array from meteorological sources dependent on vegetation, wind speed and precipitation levels. These noise studies prove that noise is correlated in space and/or time therefore an efficient noise removal procedure must account for spatio-temporal variations of the noise field. The modelling method proposed by Birnie et al. (2016), **based on covariance modelling (Massart et al., 1988; Scharf, 1991)**, accounts for these spatio-temporal variations by generating multivariate Gaussian distributions whose defining statistics are derived to be identical to that of the observed noise. A single-variate Gaussian distribution is uniquely described by a single mean and standard deviation while a multi-variate Gaussian distribution is described by its mean vector and the lower triangular part of the Cholesky decomposition of its covariance matrix. In this section we describe how to estimate the covariance from recorded data and subsequently remove the covariance from a recorded time series.

To compute the covariance matrix the seismic recording is split into multiple realisations, where a realisation is a time segment of the data. Following the first five steps of the noise

modelling procedure (Birnie et al., 2016), the realisations are reshaped into column vectors, \mathbf{d}_i , and the sample mean for each time-space point is removed (i.e. $\hat{\mathbf{d}} = \mathbf{d} - \boldsymbol{\mu}$). The covariance, \mathbf{C} , is computed using

$$\mathbf{C} = \hat{\mathbf{D}}\hat{\mathbf{D}}^T/K, \quad (1)$$

where $\hat{\mathbf{D}} = [\hat{\mathbf{d}}_1 \ \hat{\mathbf{d}}_2 \ \dots \ \hat{\mathbf{d}}_{K-1} \ \hat{\mathbf{d}}_K]$, $\hat{\mathbf{D}}^T$ is the transpose of $\hat{\mathbf{D}}$ and K is the number of realisations. The covariance matrix is then decomposed into its upper and lower triangular matrices using a Cholesky decomposition,

$$\mathbf{C} = \mathbf{C}^{1/2}(\mathbf{C}^{1/2})^T, \quad (2)$$

where $\mathbf{C}^{1/2}$ is the lower triangular matrix. To whiten the noise, the inverse of the lower triangular matrix is multiplied by a realisation of recorded data, \mathbf{x} , and scaled by α , the average of the diagonal elements of \mathbf{C} ,

$$\tilde{\mathbf{x}} = \frac{\mathbf{C}^{-1/2}\mathbf{x}}{\alpha}, \quad (3)$$

to return the data to having an identity covariance matrix. **To get an accurate estimate of the data's covariance matrix, realisations should have similar statistical properties.**

The underlying principle behind the noise whitening procedure is that the noise in the data sample, \mathbf{x} , can be effectively represented by the covariance matrix, \mathbf{C} , and will be transformed into a random sequence (for example Hom and Johnson, 1985; Belouchrani et al., 1997; Kessy et al., 2015). However, the signals in \mathbf{x} we wish to preserve will be invariants of $\mathbf{C}^{1/2}$ and hence be preserved.

3. Methodology

The removal of the covariance has to be performed over the same time length as that of the realisations used to compute it. **However recordings last significantly longer than the**

realisation lengths therefore, for practical purposes, we would require to attenuate noise over much longer periods, we approach this problem in two ways - the first is to separate the data for noise whitening into the realisation length, perform the noise whitening on each data realisation and concatenate the data segments back together. We refer to this as independent patch whitening. The second approach is to overlap the data realisations for noise whitening and then use a Hanning window to taper the patches for the concatenation. The independent patch whitening procedure (referred to as IPW hereafter) forms the basis methodology for the paper and the two extension procedures discussed in this paper - rolling noise whitening procedure (referred to as RNW hereafter) and a rolling covariance whitening procedure (referred to as RCW hereafter). The steps for IPW are given in Figure 1.

RNW is an extension of IPW by overlapping noise realisations in steps 5 and 6. This is done by extending the realisation length for both \mathbf{d} and \mathbf{x} in steps 2 and 5 and allowing realisations to overlap at the start and end of each patch. In step 6 when the whitened data is reshaped back to the original dimensions this is done using a Hanning window taper as illustrated in figure 2.

The final extension to the whitening procedure incorporates a rolling covariance calculation into the RNW procedure, resulting in the RCW procedure. This involves reassigning \mathbf{d} at predetermined points in \mathbf{x} to be the data directly preceding that point in \mathbf{x} . Then steps 2-4 are repeated on the updated data \mathbf{d} prior to continuing with the rolling noise whitening.

In this study we have used 3.5 minutes of noise recording to compute the covariance and 1s realisation lengths for the IPW, in accordance with the size and number of realisations used to compute the covariance matrix in the modelling method of (Birnie et al., 2016). For RNW and RCW a realisation length of 1.2s is used, allowing a 0.1s 'buffer' either side of the realisation. Therefore, the taper transitions are 0.2s in length.

4. Data

The noise data utilised in this study comes from a permanent surface array installed at the Aquistore carbon dioxide (CO₂) storage site, located in South Saskatchewan, Canada in the northern part of the Williston Basin (Roach et al., 2015). The array consists of 51 buried, vertical component geophones with a cross-shaped geometry as illustrated in Figure 3. The geophones are 10Hz instruments buried at a depth of 20m with a sampling frequency of 500Hz. The noise is extracted from an hour recording beginning at 14:00 local time on 7 August 2012 and **includes stationary noise signals observed constantly across the full recording, non-stationary noise signals rarely observed and pseudo-non-stationary noise signals observed for the majority of the recording however not constantly (for detailed explanation refer to Birnie et al. (2016)).** Examples of the noise used are given in Figure 4, **where heightened noise levels are observed around the centre of the array.**

Synthetic waveform data has been used in this study to identify the effect the noise balancing procedure has on signals from microseismic events. The waveform data is generated using E3D (Larsen and Harris, 1993). The source is placed below the middle of the N-S/E-W cross-shaped array at a depth of 1.6km, where the subsurface is modelled as a 16-layer, laterally homogeneous, isotropic medium with properties as described by Roach et al. (2015). A point source with a central frequency of 30Hz has been used to remove any requirement for polarity correction during the imaging of the event. The synthetic waveform data is used independently as well as combined with the recorded noise to make semi-synthetic datasets. ~~as illustrated in Figure ??b.~~ When creating semi-synthetics the SNR is determined by the ratio of the maximum amplitudes of the noise and waveform data.

5. Results

5.1. Noise whitening

The noise data used to compute the covariance matrix and the noise to be whitened are given in Figure 4a and b, respectively. Figure 5a and b illustrate the results from IPW where the data to be whitened has been split into 1s realisations prior to removal of the covariance. We see that the noise energy has been successfully distributed across the receiver array by the whitening procedure. As detailed in table 1, the total energy across the array has decreased by 65% with the noisiest station (i.e. station 41) experiencing an energy decrease of 89% and the quietest station still experiencing an energy decrease by 15%. A notable feature of figure 5b is the significant edge effects which occur at the beginning of each patch in the denoised data (shown as black arrows in the figure). Due to these effects the change in noise levels is calculated from 0.2s in the data window.

Figure 5c and d illustrate the results from RNW. While the patch transitions still occur at the same location, the tapering procedure has removed all noticeable edge effects. To provide direct comparison with the IPW, the second row of table 1 is the sum of energy from 0.2 – 1s while the final row is the sum of energy for the full 6s of data. As with IPW, RNW successfully distributes the energy across the array decreasing the total noise level of the 6s of data by 84%. The noise energy at station 41 decreased by 90% while station 50 decreased by 13%. Changes in the values by which the noise decreases between IPW and RNW can be attributed to them using different lengths of realisations in the computation of the covariance matrix. **Due to the suppression of the edge effect, RNW is the better of the two techniques.**

The power spectrum of station 41 prior to whitening and after RNW is given in Figure 6. While there is not equal amounts of power in each frequency band, the power spectrum for the whitened data is significantly flatter with less energy in the lower frequencies and more in the higher frequencies than that of the noise prior to whitening.

5.2. Effect on arrival observations

To analyse the effect of noise whitening on a signal from a microseismic event RNW was performed on a semi-synthetic dataset and on noise-free synthetic waveform data, illustrated in figure 7. **The noise used to create the semi-synthetic dataset is the same as the noise whitened in the previous section.** In the semi-synthetic case we see that the arrival is clearly retrieved by the denoising procedure, and the residual/noise section is overwhelmingly dominated by the removed noise. **Due to the long period nature of the noise, the whitening process has acted similar to that of a high pass filter on some traces however it has done so automatically and with reference to the phase spectrum as well as the amplitude spectrum of the noise.** In the noise free synthetic application (figure 7d/e/f) we see that some of the arrival energy is attenuated by the denoising process. However, this is a negligible proportion of the amplitude **that we believe is due to the small amount of regularisation added.** Figure 8 shows the change in power spectrum and phase of station 41 for the first arrival ($0 < t < 0.4\text{s}$) of the noise-free data before and after whitening. We find that between frequencies 10 to 70Hz there is close match in both energy content and phase of the first arrival. It should be noted that the input wavelet is a 30Hz Ricker wavelet and therefore has a very limited amount of energy outside the 10-70Hz range (note the log scale in figure 8).

Diffraction stack imaging was performed on the semi-synthetic data prior to and after whitening to identify the benefits whitening has on event location determination. Figure 9 shows that at a SNR of 0.04 the image maxima for the original data is an artefact arising from the noise in the dataset however when noise whitening has been applied these artefacts are significantly reduced resulting in the image maxima correctly locating the seismic event. At a SNR of 0.08 both the original data and whitened data have a maxima at the seismic source location however there is still significant energy from the noise creating artefacts in the image while there are no noise artefacts in the whitened data image.

5.3. Robustness tests

As discussed in detail in Birnie et al. (2016) study, to get a usable covariance matrix for modelling it is required that the realisations used to create the covariance have the same statistical properties. The following results are to test the extent to which this holds for the noise whitening case, i.e. to test the extent to which the noise can vary within both the dataset for computing the covariance and for whitening. The first scenario tested, Scenario 1, has a change in noise type at approximately 3s into the data from a regime consistent with the data used to estimate the covariance matrix to one where a dominant source of noise for several traces is absent (figures 10a - c). Despite a very minor increase in the whitened noise level at the transition between the two noise signals, the noise whitening procedure is successful, reducing the noise by 84% (table 2). Scenario 2, figures 10d - f, considers where there the data used to construct the covariance matrix contains examples of the desired signals. In this case we use a swarm of 20 microseismic events, alongside a change in noise type. The whitened data appears unaffected by the signals or the changing noise types.

The final two scenarios utilise a high amplitude noise burst resulting from a passing car. In scenario 3, the car energy is placed in the data used to compute the covariance (figures 10g - i). Visually the results show that the high energy noise burst has little to no effect on the whitening procedure however the energy at station 13 has increased by 163% showing that the whitening does not perform as well on the stations affected by the noise burst. In scenario 4, the car energy is placed in the data to be whitened. Note that as the duration of the burst is longer than the duration of the traces in figures 10k and l it appears as a vertical stripe on traces 11 – 15. The background noise has been whitened with station 41 experiencing a reduction in noise energy by 73% yet the high-energy noise due to the car has not been suppressed.

5.4. Extension: Rolling covariance calculation

An extension to the noise whitening procedure is RCW where the covariance matrix is updated/recomputed using a rolling window of 3.5 minutes of data prior to the data sample to be denoised. Ten minutes of data have been whitened with the covariance matrix being recalculated every 5s. Due to the size of the covariance matrix it is not possible to save them and compare the differences for every 5s therefore an event has been added at ~ 2.5 s into each patch and the SNR is calculated before and after whitening. Figure 11a shows the SNR of each 5s patch after whitening and compares it with the difference for the case where a single covariance was used for whitening the full 10minutes (i.e. RNW case), while Figure 11b shows the change in SNR after whitening for both RNW and RCW. The RNW and RCW perform very similarly, with both techniques struggling with high energy noise at approximately 3.25 and 8.6 minutes similar to the noise observed in robustness scenarios 3 and 4, and neither significantly outperform the other in increasing the SNR through whitening.

6. Discussion

In essence, noise whitening has been shown to increase SNR by randomisation of the noise. Comparing the mean noise energy of 1s on stations 1 and 41 (i.e. a ‘quiet’ and ‘noisy’ station), prior to whitening station 41 is ~ 5 times noisier than station 1, while after whitening that is reduced to ~ 3 times. Whilst the noise has been whitened it has also been reduced in amplitude with station 1 experiencing a decrease of $\sim 50\%$ and station 41 experiencing a decrease of $\sim 71\%$. While there are still observable changes in the noise levels across the array, they have been significantly reduced through whitening.

The majority of noise suppression techniques are directed approaches in which noise with a particular property is removed. For example, suppressing noise with a linear moveout (e.g. Forghani-Arani, 2013) or suppressing noise with a particular slowness (e.g. Roux et al., 2014; Dando et al., 2016). As these techniques are based on exploiting a property of the

noise they therefore require knowledge of the noise's properties to effectively suppress it. The technique proposed in this paper is an example of an undirected approach which makes no assumptions on the noise's origin or the form it takes within the data. An example of another undirected approach is that of Blunda and Chambers (2013) whose combination of time-frequency winsorisation and adaptive subtraction procedures result in a modest SNR gain of 4-12 dB.

Not only does the noise whitening technique make no assumptions on the noise but it has been shown to provide a clean separation between signal and noise even when signals are present within the data used to compute the covariance matrix. In general, the signals of interest are very short in duration and few in number relative to the noise. Therefore when the covariance is computed the signals are averaged out by the noise resulting in a covariance matrix that models the noise with very little contribution from the signals. Provided the seismic arrivals are invariants of the covariance matrix then they are unaffected by the whitening procedure.

Whitening the data resulted in better imaging of lower SNRs without any additional processing. A benefit of this procedure is that once the covariance has been computed, the incoming data can be processed in real time, with each new patch recorded being whitened prior to the use of automated detection and location procedures. The results from the robustness tests showed that the noise whitening procedure continues to work effectively where there are significant noise variations between patches used to compute the covariance matrix, i.e. scenarios 2 and 3, as well as where there are noise variations within the data for whitening, scenario 1. However, from experience it is worth noting that to ensure the covariance represents the majority noise signal then it should be present in approximately 50% of the patches. Our results also show that the high contrast between the base noise signal and the passing car in the final scenario results in the car noise not being whitened. For single high-energy bursts that affect a small number of receivers there are alternative methods

for noise suppression, such as despiking in the time-frequency domain, which we would encourage to be used after noise whitening to remove such signals that cannot be suppressed during whitening. When combining the noise whitening procedure with diffraction stack imaging, events were detected at SNR 50% lower than without noise whitening, highlighting the benefits of performing noise whitening prior to random noise attenuation techniques.

The last section of the results focusses on extending the technique to include a rolling covariance calculation from the 3.5 minutes of data directly preceding the data for whitening. If a site experiences significantly changing noise, with respect to time, then the recalculation of the covariance may be worthwhile however in this case the noise was deemed sufficiently stable to provide any benefits from continually updating the covariance matrix. Other extensions to this study could include computing a covariance matrix of a single noise type and use that to whiten only that noise type.

On a concluding note, while this paper has focussed on the application to surface microseismic this technique is applicable to any time series recording where noise can be considered as a multivariate Gaussian distribution. Future studies should focus on the benefits this technique can bring to other exploration, global and hazard monitoring applications.

7. Conclusions

In this study we have shown that noise whitening provides a robust method for increasing SNR in surface seismic data. Applicable in any situation with one or more receivers, this method has the ability to be used after data has been collected or continually on new data as it is being recorded, and as a pre-cursor to random noise attenuation procedures or as a stand-alone method. Noise whitening has a negligible effect on a seismic wavelet whilst significantly reducing noise energy resulting in improved event detection and imaging at lower SNR than originally possible. For the microseismic monitoring scenario, the ability to push the imaging capabilities to significantly lower SNR will allow improved characterisation

of fracture systems, due to the higher number of low energy events in comparison to the lower number of high energy events (Gutenberg and Richter, 1944). The technique performs exceptionally well in robustness tests on data experiencing varying noise properties, reducing the noise energy by at least 23% even when there are noise signals present that are not whitened, such as spurious high energy bursts. In this paper we have demonstrated that noise whitening is a powerful and flexible noise attenuation method, and as such is a valuable addition to the geophysicists toolbox.

Acknowledgements

The authors would like to thank Frans Kets for valuable discussions during this study. We would like to thank the Petroleum Technology Research Centre (PTRC) for access to Aquistore Data. Aquistore an independent research and monitoring project managed by the PTRC which intends to demonstrate that storing liquid carbon dioxide (CO₂) deep underground (in a brine and sandstone water formation), is a safe, workable solution to reduce greenhouse gases (GHGs). C. Birnie is funded by the NERC Open CASE studentship NE/L009226/1 and Pinnacle-Halliburton. D. Angus acknowledges the Research Council UK (EP/K035878/1; EP/K021869/1; NE/L000423/1) for financial support.

References

- Auger, E., Schissel -Rebel, E., Jia, J., 2013. Suppressing noise while preserving signal for surface microseismic monitoring: The case for the patch design. In: 2013 SEG Annual Meeting. Society of Exploration Geophysicists.
- Belouchrani, A., Abed-Meraim, K., Cardoso, J.-F., Moulines, E., 1997. A blind source separation technique using second-order statistics. *IEEE Transactions on signal processing* 45 (2), 434–444.

- Bensen, G., Ritzwoller, M., Barmin, M., Levshin, A., Lin, F., Moschetti, M., Shapiro, N., Yang, Y., 2007. Processing seismic ambient noise data to obtain reliable broad-band surface wave dispersion measurements. *Geophysical Journal International* 169 (3), 1239–1260.
- Birnie, C., Chambers, K., Angus, D., Stork, A., August 2016. Analysis and models of pre-injection surface seismic array noise recorded at the aquistore carbon storage site. *Geophysical Journal International* 206 (2), 1246–1260.
- Blunda, Y., Chambers, K., 2013. A methods procedure for noise suppression in microseismic data. In: CSPG/CSEF/CWLS Geo Convention.
- Dando, B., Iranpour, K., Oye, V., Bussat, S., Bjerrum, L., 2016. Real-time microseismic monitoring in the north sea with advanced noise removal methods. In: SEG Technical Program Expanded Abstracts 2016. Society of Exploration Geophysicists, pp. 2657–2661.
- Eisner, L., Abbott, D., Barker, W. B., Thornton, M. P., Lakings, J., 2008. Noise suppression for detection and location of microseismic events using a matched filter. In: 2008 SEG Annual Meeting. Society of Exploration Geophysicists.
- Forghani-Arani, F., 2013. Analysis and suppression of passive noise in surface microseismic data. Ph.D. thesis, Colorado School of Mines.
- Forghani-Arani, F., Batzle, M., Behura, J., Willis, M., Haines, S. S., Davidson, M., 2012. Noise suppression in surface microseismic data. *The Leading Edge* 31 (1496–1501), 1496–1501.
- Gambino, S., Mostaccio, A., Patanè, D., Scarfi, L., Ursino, A., 2004. High-precision locations of the microseismicity preceding the 2002–2003 mt. etna eruption. *Geophysical research letters* 31 (18).
- Gutenberg, B., Richter, C. F., 1944. Frequency of earthquakes in california. *Bulletin of the Seismological Society of America* 34 (4), 185–188.

- Hom, R. A., Johnson, C. R., 1985. Matrix analysis. Cambridge University Express.
- Kessy, A., Lewin, A., Strimmer, K., 2015. Optimal whitening and decorrelation. eprint arXiv:1512.00809.
- Larsen, S., Harris, D., 1993. Seismic wave propagation through a low-velocity nuclear rubble zone. Tech. rep., Lawrence Livermore National Lab., CA (United States).
- Massart, D. L., Vandeginste, B., Deming, S., Michotte, Y., Kaufman, L., 1988. Chemometrics: a textbook.
- Maxwell, S., 2010. Microseismic: Growth born from success. *The Leading Edge* 29 (3), 338–343.
- Maxwell, S., 2011. Microseismic hydraulic fracture imaging: The path toward optimizing shale gas production. *The Leading Edge* 30 (3), 340–346.
- Nørmark, E., 2011a. Suppression of traffic noise on vibroseismic data. In: *Near Surface 2011-the 17th European Meeting of Environmental and Engineering Geophysics*.
- Nørmark, E., 2011b. Wind and rain induced noise on reflection seismic data. In: *Near Surface 2011-the 17th European Meeting of Environmental and Engineering Geophysics*.
- Oye, V., Aker, E., Daley, T. M., Kühn, D., Bohloli, B., Korneev, V., 2013. Microseismic monitoring and interpretation of injection data from the in salah co 2 storage site (krechba), algeria. *Energy Procedia* 37, 4191–4198.
- Roach, L. A., White, D. J., Roberts, B., 2015. Assessment of 4d seismic repeatability and co2 detection limits using a sparse permanent land array at the aquistore co2 storage site. *Geophysics* 80 (2).
- Roux, P.-F., Kostadinovic, J., Bardainne, T., Rebel, E., Chmiel, M., Van Parys, M., Macault, R., Pignot, L., 2014. Increasing the accuracy of microseismic monitoring using surface patch arrays and a novel processing approach. *first break* 32 (7), 95–101.

- Scharf, L. L., 1991. Statistical signal processing. Vol. 98. Addison-Wesley Reading, MA.
- Schilke, S., Probert, T., Bradford, I., Özbek, A., Robertsson, J., 2014. Use of surface seismic patches for hydraulic fracture monitoring. In: 76th EAGE Conference and Exhibition 2014.
- Schorlemmer, D., Wiemer, S., 2005. Earth science: Microseismicity data forecast rupture area. *Nature*.
- Staněk, F., Eisner, L., Jan Moser, T., 2014. Stability of source mechanisms inverted from p-wave amplitude microseismic monitoring data acquired at the surface. *Geophysical Prospecting* 62 (3), 475–490.
- Wang, J., Tilmann, F., White, R., Soosalu, H., Bordononi, P., 2008. Application of multichannel wiener filters to the suppression of ambient seismic noise in passive seismic arrays. *The Leading Edge* 27 (2), 232–238.
- Yilmaz, Ö., 2001. Seismic data analysis. Vol. 1. Society of Exploration Geophysicists Tulsa.
- Zhebel, O., Gajewski, D., Vanelle, C., 2011. Localization of seismic events in 3d media by diffraction stacking. In: 73rd EAGE Conference & Exhibition.

8. Tables and figures

		Total energy		
		Station 41	Station 50	Full array
Individual patch whitening (0.8s)	Before	0.0682	0.0071	0.7721
	After	0.0076	0.0060	0.0942
	%Change	89	15	65
Rolling noise whitening (0.8s)	Before	0.0682	0.0071	0.7721
	After	0.0097	0.0051	0.1138
	%Change	86	28	62
Rolling noise whitening (6s)	Before	0.5769	0.0464	4.7236
	After	0.0553	0.0405	0.7405
	%Change	90	13	84

Table 1: Change in noise energy before and after noise whitening for a noise station (Station 41), a quiet station (Station 50) and the full array. To minimise the influence of the edge effect, the first two rows are calculated from 0.2 – 1s. The final row is calculated for full 6s of whitened data.

		Total energy		
		Station 41	Station 13	Full array
Scenario 1	Before	0.1721	0.0023	1.8732
	After	0.0187	0.0021	0.3052
	%Change	89	9	84
Scenario 2	Before	0.1647	0.0032	1.6527
	After	0.0252	0.0022	0.2974
	%Change	85	31	82
Scenario 3	Before	0.1647	0.0032	1.6527
	After	0.0204	0.0084	0.3209
	%Change	88	163 (Inc.)	81
Scenario 4	Before	0.1389	1.9229	3.8383
	After	0.0377	2.1322	2.9425
	%Change	73	10 (Inc.)	23

Table 2: Change in noise energy before and after whitening for multiple scenarios tested.

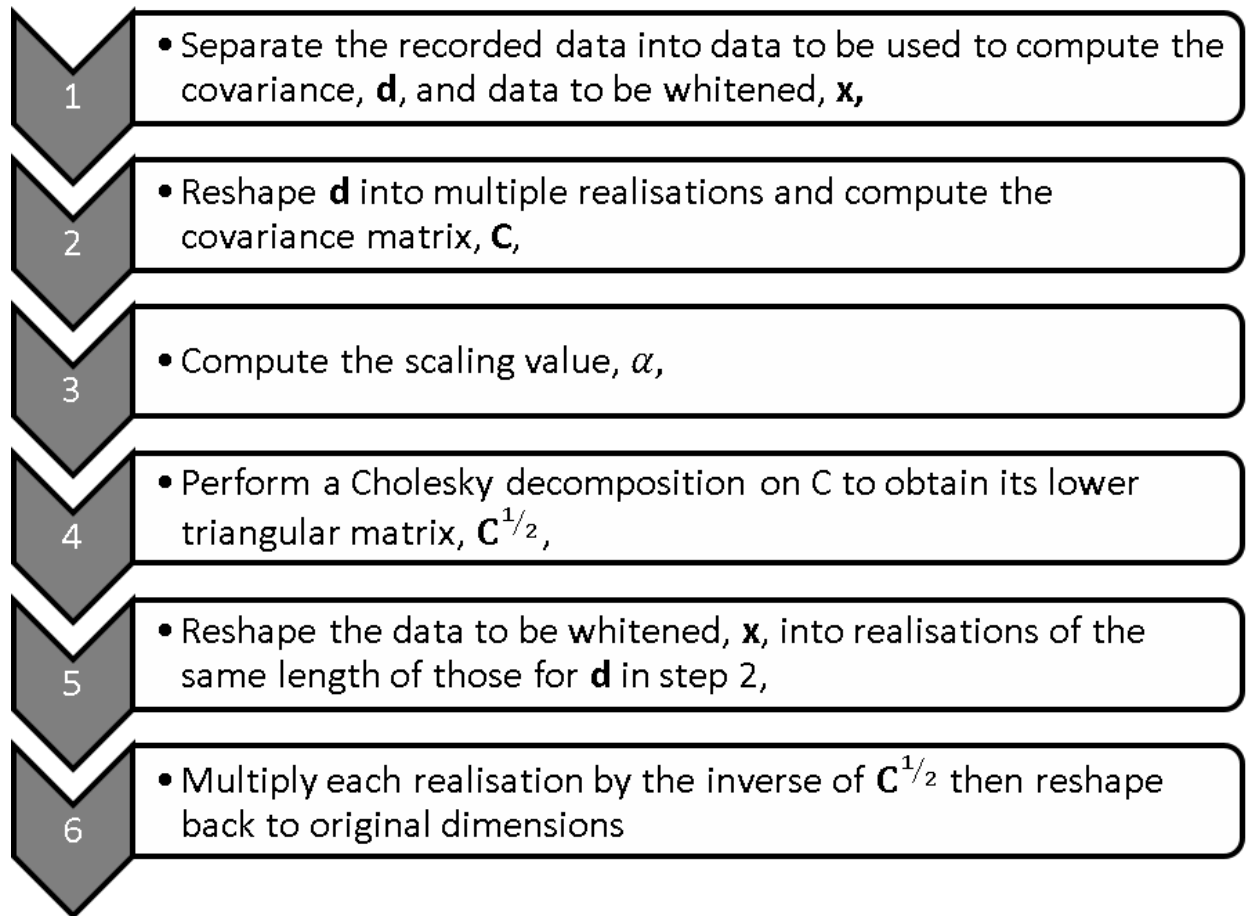


Figure 1: Workflow of Independent Patch Whitening method.

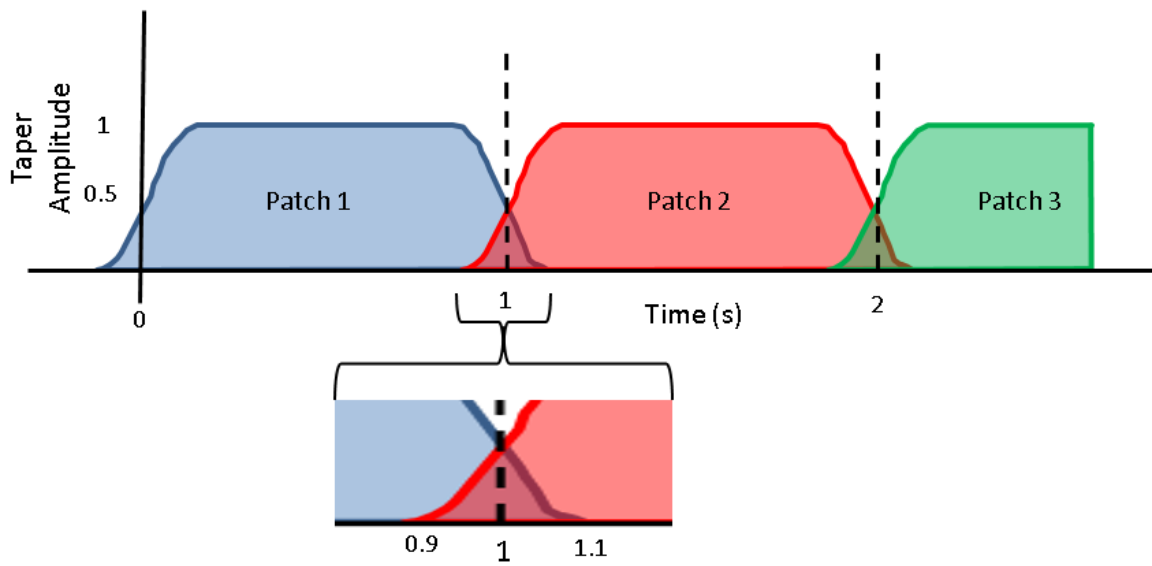


Figure 2: Schematic of taper filters used for rolling noise whitening.

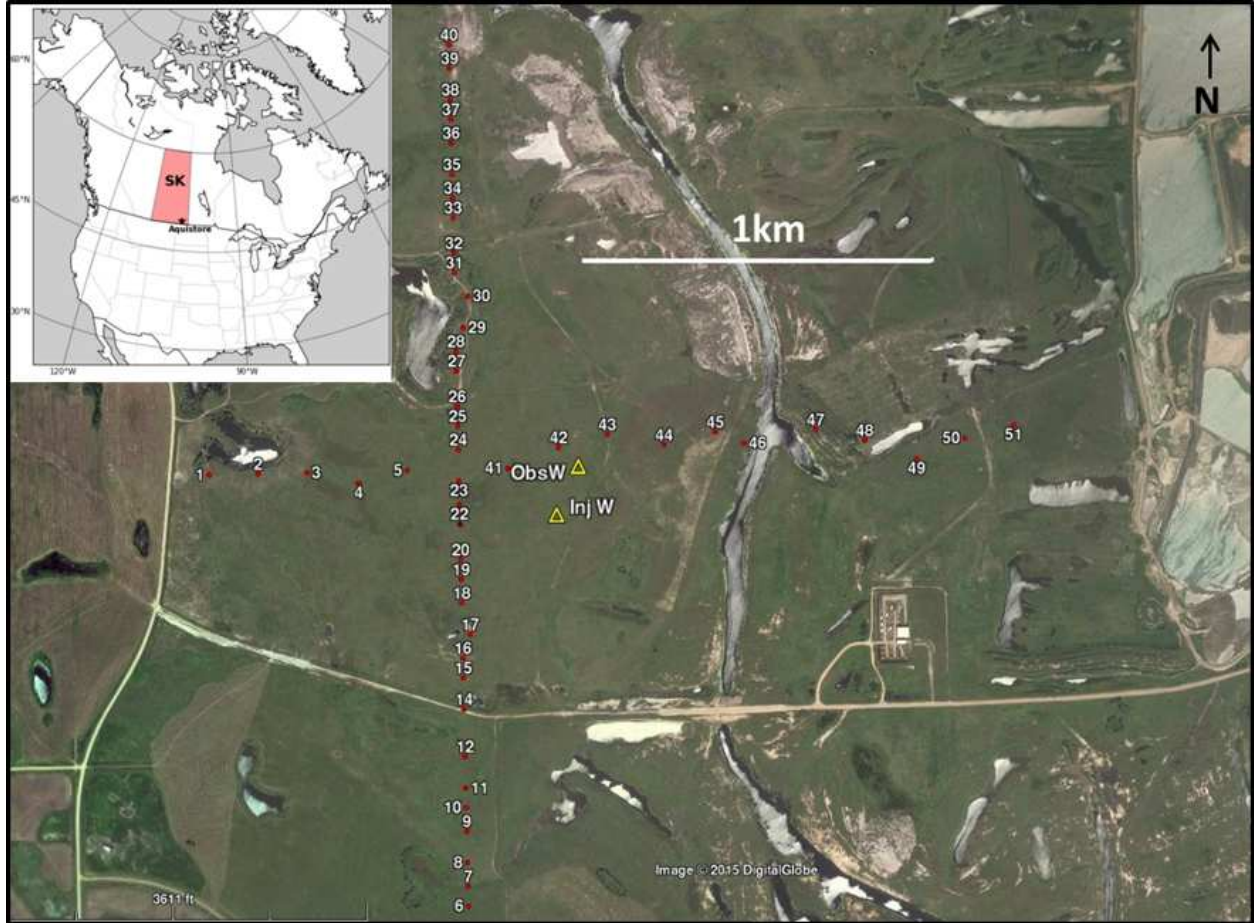


Figure 3: Aquistore permanent seismic array survey geometry. Geophones are denoted by red dots alongside the station number, while the observation and injection wells are illustrated by yellow triangles.

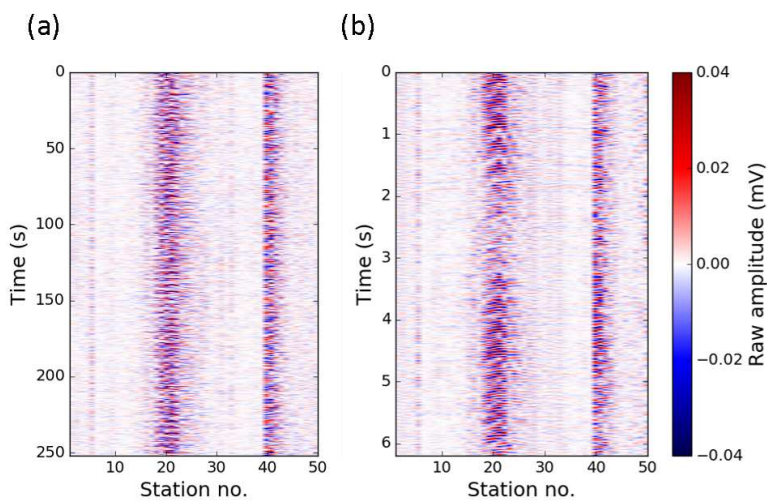


Figure 4: (a) Noise data for computing covariance matrix and (b) noise data to be whitened.

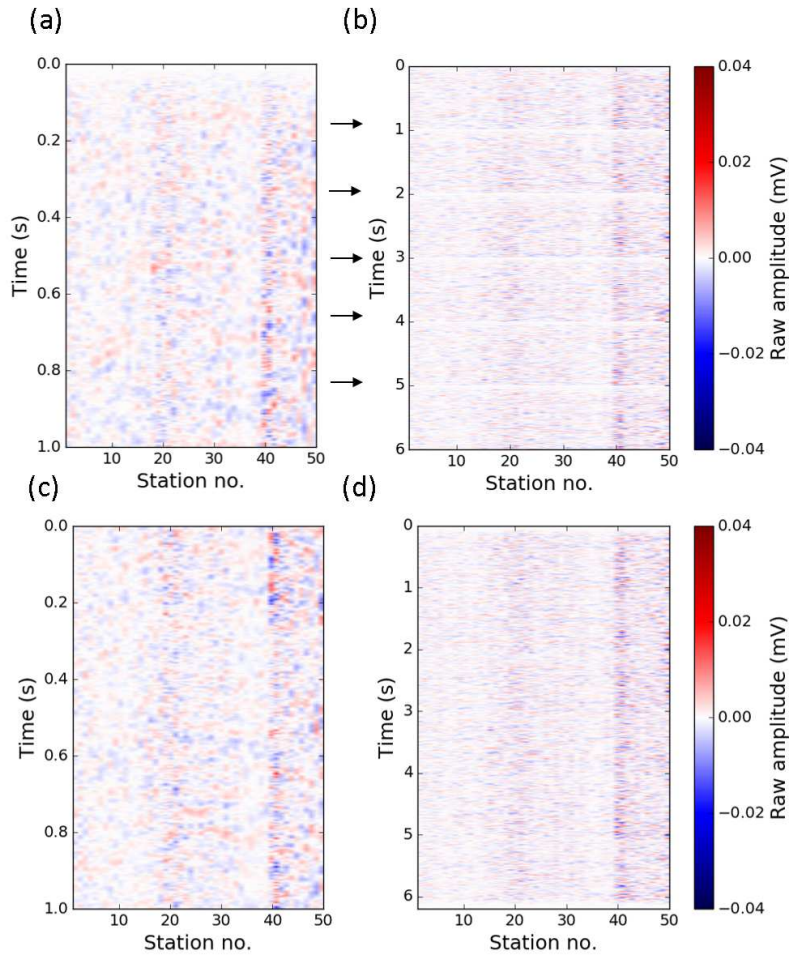


Figure 5: Whitened noise data, (a) and (b) using independent patch method, IPW, (c) and (d) using rolling noise method, RNW. (a) and (c) are 1s segments of the 6s of whitened data (b) and (d). Black arrows indicate edge effect from IPW.

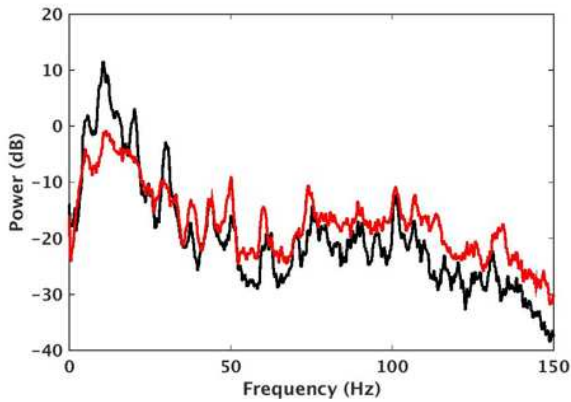


Figure 6: Power spectrum of noise data at station 41 before (black) and after (red) whitening.

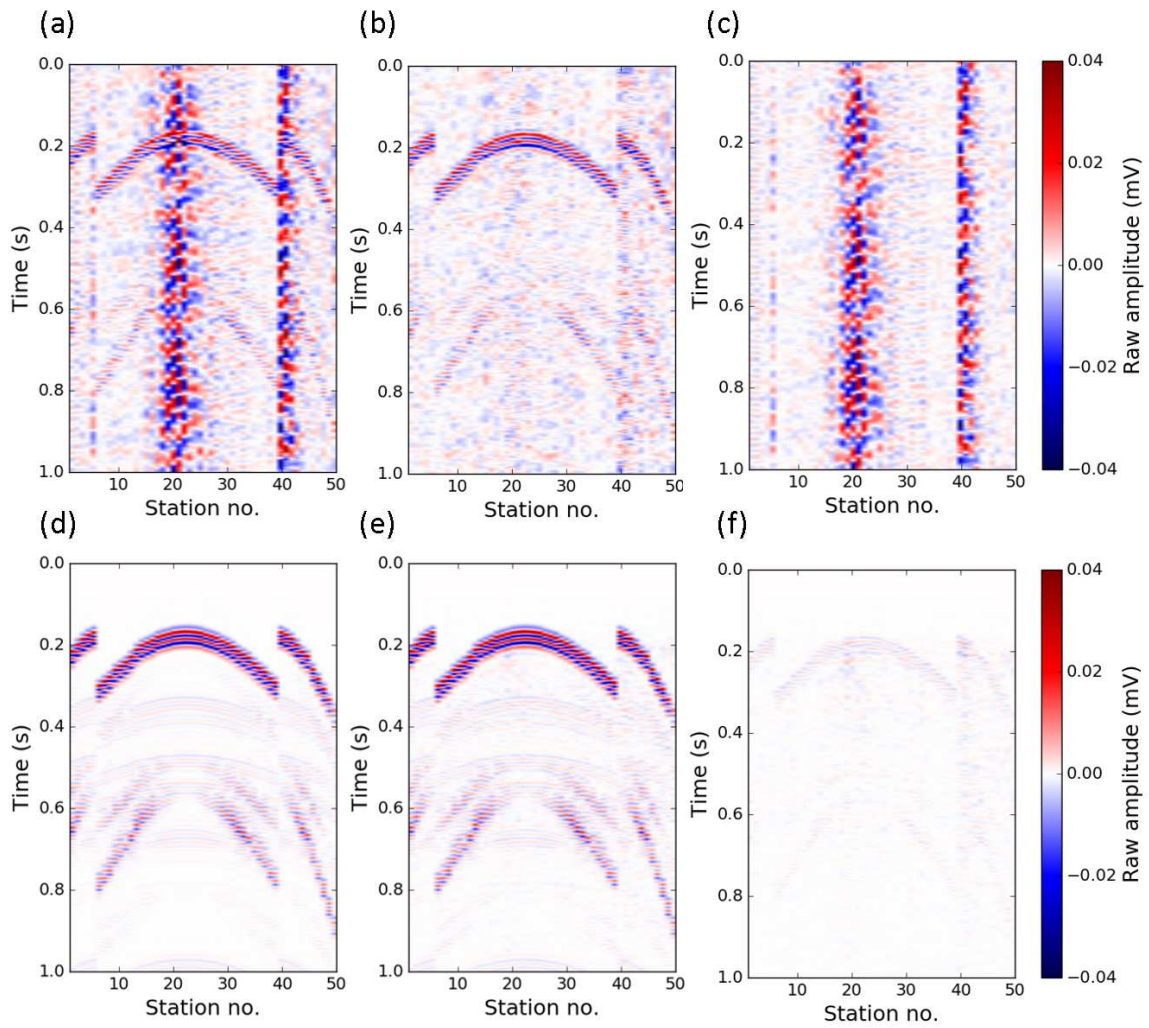


Figure 7: Semisynthetic (a) before and (b) after whitening and (c) the difference between the two. And a noise-free event (d) before and (e) after whitening and (f) the difference between the two.

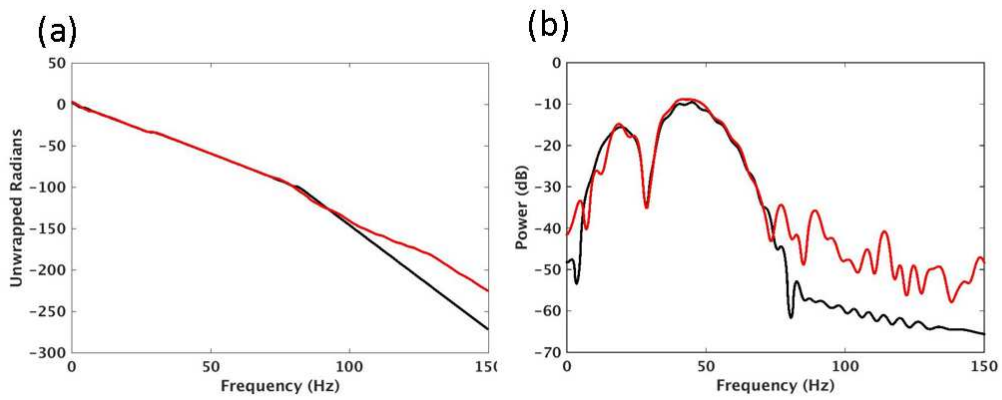


Figure 8: (a) Phase and (b) power spectra of first arrival at station 41 from noise-free event before (black) and after (red) whitening. Note the logarithmic scale used in (b).

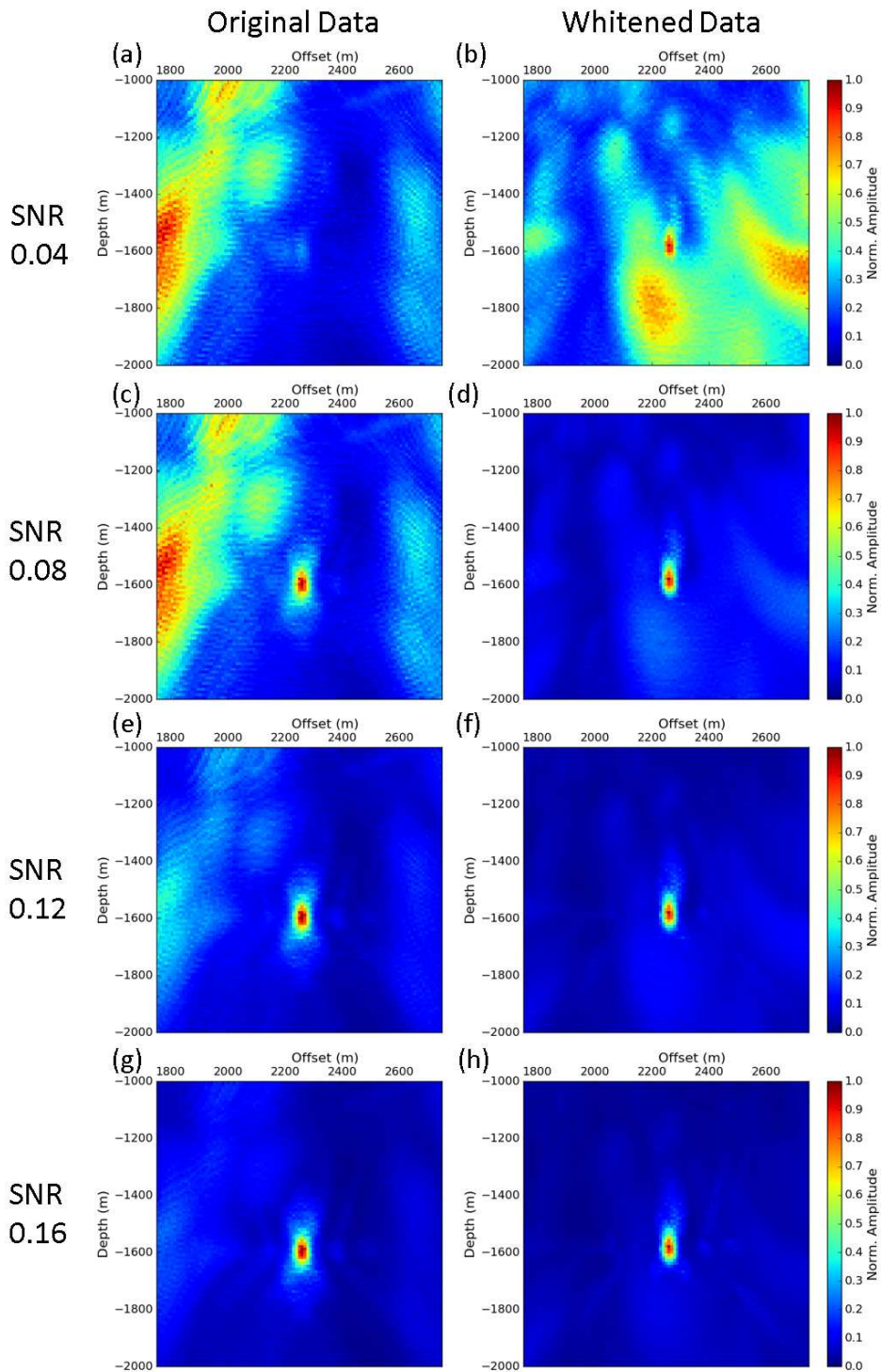


Figure 9: Diffraction stack imaging of microseismic event at 1.6km depth and 2260m offset for SNR of semisynthetic datasets before (first column) and after whitening (second column) at increasing SNRs.

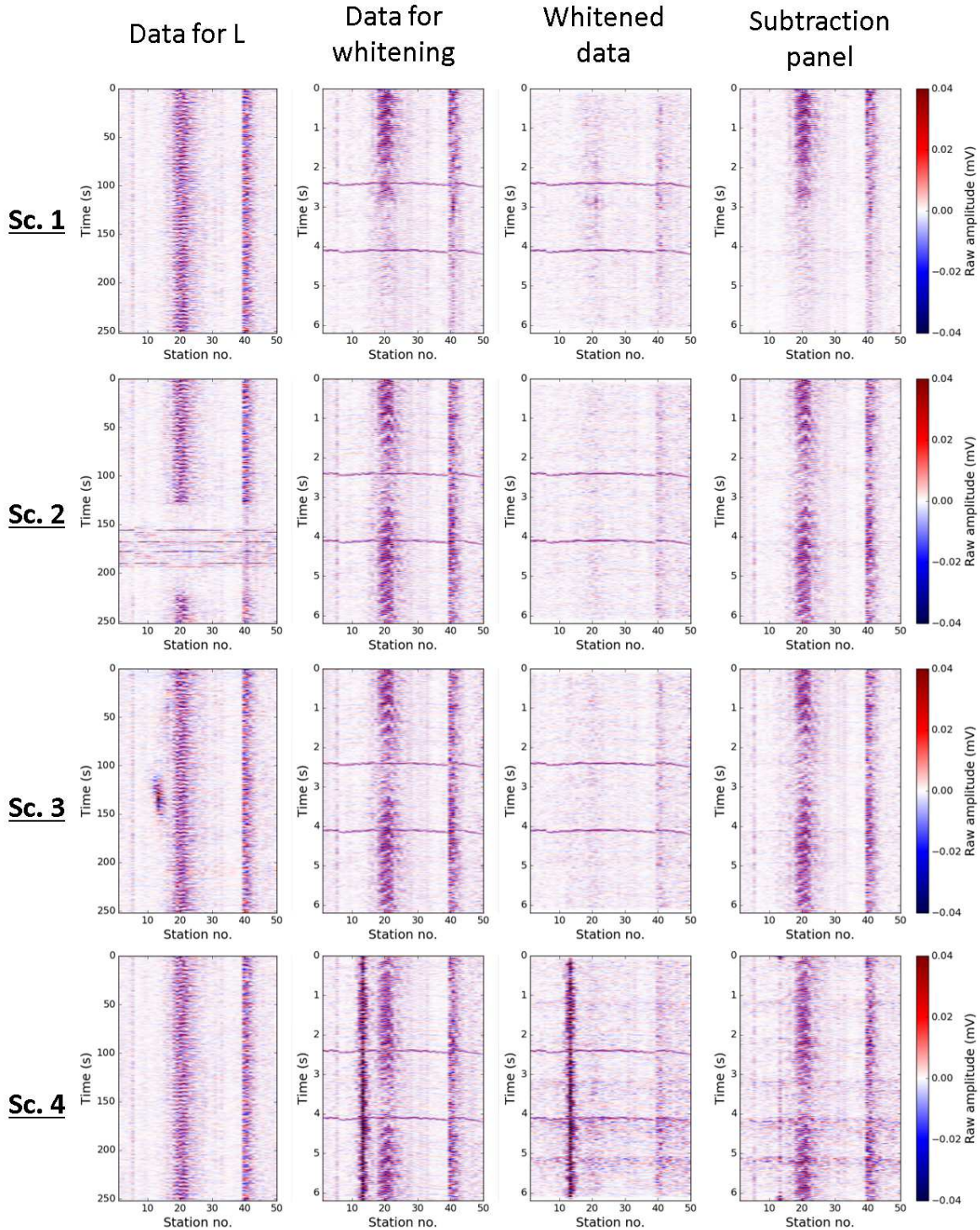


Figure 10: Robustness tests. Scenario 1 involves a change in noise properties in data for whitening; Scenario 2 involves a change in noise and swarm of 20 events in data used to compute L ; Scenario 3 involves a high-energy noise burst in data used to compute L ; and, scenario 4 involves a high-energy noise burst in data for whitening. The first column is data to compute the covariance, the second is data to be whitened, the third is whitened data and the fourth column is the difference between the second and third.

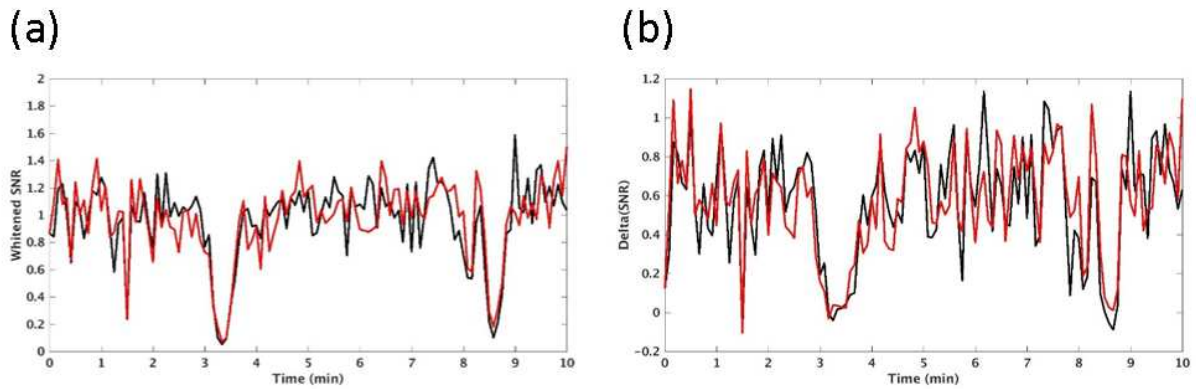


Figure 11: (a) Comparison of SNR of 5s data patches after whitening for RNW (black line) and RCW (red line), where the covariance matrix is recomputed every 5s, and (b) change in SNR (i.e. $\Delta(\text{SNR})$) before and after whitening, where negative delta corresponds to an increase in SNR after whitening.